JOURNAL OF MATERIALS SCIENCE 37 (2002) 3163–3173

Calcium aluminate cements in fly ash/calcium aluminate blend phosphate cement systems: Their role in inhibiting carbonation and acid corrosion at a low hydrothermal temperature of 90°C

T. SUGAMA
Brookhaven National Laboratory, Energy Resources Division, Energy Science and Technology Department, Upton, NY 11973, USA
E-mail: sugama@bnl.gov

L. E. BROTHERS
Halliburton, 2600 S. 2nd Street, Duncan, OK 73536-0442, USA

L. WEBER
Unocal Corporation, 1414 Southwest Freeway, Sugar Land, TX 77478, USA

Study was focused upon formulating sodium polyphosphate-modified fly ash/calcium aluminate blend (SFCB) geothermal well cements with advanced anti-carbonation and anti-acid corrosive properties. At a low hydrothermal temperature of 90°C, to improve these properties, we investigated the effectiveness of various calcium aluminate cement (CAC) reactants in minimizing the rate of carbonation and in abating the attack of H_2SO_4 (pH ~ 1.6). We found that the most effective CAC had two major phases, monocalcium aluminate (CA) and calcium bialuminate (CA_2), and a moderate CaO/Al_2O_3 ratio of 0.4. The reaction between sodium polyphosphate (NaP) and CA or CA_2 at room temperature led to the formation of amorphous dibasic calcium phosphate hydrate and anionic aluminum hydroxide caused by the decalcification of CA and CA_2. When SFCB cement made with this CAC was exposed to 4% $NaHCO_3$-laden water at 90°C, some carbonation of the cement occurred, forming calcite that was susceptible to the reaction with H_2SO_4. This reaction resulted in the deposition of gypsum gel scales as the acid corrosion product on the cement surfaces. The scale layer clinging to the cement protected it from further corrosion. Under such protection, the amorphous dibasic calcium phosphate hydrate → crystal hydroxyapatite and anionic aluminum hydroxide → crystal boehmite phase transitions were completed in acid solution. Meanwhile, the further chemical and hydration reactions of NaP with fly ash led to the formation of additional crystalline Na-P type zeolite phases. Thus, we propose that passivation of the surface of the cement by deposition of gypsum, following the formation of these reaction products, which are relatively inert to acid, are the acid corrosion-inhibiting mechanisms of the SFCB cements.

1. Introduction

Cement for geothermal wells was developed and formulated at Brookhaven National Laboratory (BNL) in collaboration with two industrial partners, Unocal Corporation and Halliburton Energy Services [1, 2]. This cement met the following six criteria: (1) compatible with conventional field placement technologies; (2) formed water-soluble carbonates <5 wt% after 1 year in brine at 300°C containing ~40,000 ppm CO_2; (3) compressive strength >5 MPa at 24 hr age; (4) pumpability of ~4 hr at 50°C; (5) bond strength to steel >70 KPa; and (6) water permeability <0.1 mDarcy. The chemical components of the developed cement consisted of calcium aluminate cement (CAC), Class F fly ash as a recycled byproduct of coal combustion, sodium polyphosphate as fertilizer intermediate, and water. This cement was prepared by an acid-base reaction between sodium polyphosphate solution as an acid liquid and the Class F fly ash-blended calcium aluminate cement as a base powder reactant; this was followed by hydrothermal treatments at temperatures of up to 300°C [3]. The technology for making this sodium

polyphosphate-modified fly ash/calcium aluminate blend (SFCB) cement was transferred to two industrial collaborators, Unocal and Halliburton. Subsequent field testing and further development of the SFCB cement system by them led to full-scale tests and a field-workable cement which was first emplaced by Unocal in a geothermal well in northern Sumatra, Indonesia in September 1997. The pumping operation of cement in these wells, which was performed under the following conditions: bottomhole depth of 1680 m, downhole temperature of 280°C, and CO_2 concentration of 10,000 ppm, was very successful [4]. However, one question raised concerned the resistance of SFCB cements to highly concentrated H_2SO_4 environments ($pH < 2.0$) encountered in the well's surface ground water at low temperatures around 90°C.

In our previous study on the resistance of SFCB cements to H_2SO_4 at temperature of 90°C [5], we reported that although two amorphous reaction products, $Ca(HPO_4) \cdot xH_2O$ and $Al_2O_3 \cdot xH_2O$, were responsible for alleviating acid erosion of the SFCB cements, there were two problems to be solved to confer further resistance to hot acid. One problem was the susceptibility of non-reacted calcium aluminate to H_2SO_4, and the other was the development of porous microstructure in the specimens.

Since these reaction products were formed by chemical and hydration reactions between the sodium polyphosphate solution and the calcium aluminate cement (CAC), but not fly ash, one approach to solving these problems is to understand the role of CAC reactants in the SFCB cement systems in abating acid attack. In addition, another major concern is the presence of CO_2in geothermal fluids, ranging from 20,000 to 10,000 ppm, implying that not only must the cements be resistant to acid, but also they must have little susceptibility to CO_2. Thus, it is important to know whether cements can withstand acid corrosion after being carbonated.

The focus of the present study centered on assessing the effectiveness of CAC with various mole ratios of CaO/Al_2O_3 and different mineralogical phase compositions in reducing the rates of both carbonation and acid corrosion of the SFCB cements. The factors to be assessed included loss in weight, porosity, and changes in phase composition of the carbonated cements after submersing them for 90 days in a solution of H_2SO_4, pH ~ 1.6, at 90°C. For comparison, the susceptibility of non-carbonated cements to H_2SO_4 also was investigated.

2. Experimental

We used four different-type CAC reactants, Secar 51, 60, 71, and 80, supplied by Lafarge Aluminates Corporation. The Class F fly ash with a Blaine fineness of 1.0585 m^2/g was supplied by Pozament Corp. The x-ray powder diffraction (XRD) data showed that the crystalline components of fly ash consists mainly of two major phases, mullite ($3Al_2O_3 \cdot 2SiO_2$) and quartz (SiO_2). XRD (Philips Electronic Instruments) was recorded using nickel-filtered Cu K_α radiation at 40 kV and 20 mA. A solution of 25 wt% sodium polyphosphate $-[-(-NaPO_3)_n-$, NaP] supplied by the Aldrich Chemical Company Inc., was used as the cement-forming aqueous reactant to modify the CAC and fly ash solid reactants.

The formula of the neat cement slurry was 36 wt% CAC, 24 wt% fly ash and 40 wt% (25 wt% NaP). After the three primary reactants had been thoroughly hand-mixed in a bowl for 2 min, slurry samples were cast in cylindrical molds (30 mm diam. and 70 mm long), and allowed to harden for 24 hours at room temperature. The hardened specimens were left for 24 hours in an air oven at 110°C to eliminate any free water. The dried specimens then were exposed for 20 days in 4 wt% $NaHCO_3$-laden water at 90°C to prepare the carbonated specimens. A 4 wt% $NaHCO_3$ was used to generate ~40,000 ppm CO_2 in water. Afterward, the carbonated specimens were submersed for up to 90 days in the 2 wt% H_2SO_4 solution (pH ~ 1.6) at 90°C. To maintain the pH at ~1.6, the H_2SO_4 solution was replenished with a new fresh solution every 5 days. The volume proportion of the cement specimens to the acid solution was 1 to 25. After exposure to hot acid solution, the carbonated specimens were examined to determine their changes in weight and the phase compositions assembled in the cement bodies.

For comparison, the non-carbonated SFCB cements also were exposed to acid and then were examined to obtain the same data as that described above. The identifications of phase composition and its transformation were carried out by Fourier Transform Infrared Spectroscopy (FT-IR, Perkin Elmer Model 1600) and XRD. FT-IR samples were prepared by mixing 200 mg of KBr and 3 to 5 mg of the powered sample that had been crushed to a size of <0.074 mm. The porosity of cements was determined by helium comparison pyconometry (Micromeritrics, AccuPyc 1330). The image and elemental analyses were made to explore the development of microstructure and the chemical components of the fractured surfaces of SFCB cements after exposure to acid, using scanning electron micorscopy (SEM, JEOL Model JXA-35) coupled with energy-dispersive X-ray spectrometry (EDX, Tracor Northem TN-5502).

3. Results and discussion

3.1. Chemical composition of CACs

Before exposing the SFCB cements to hot $NaHCO_3$-laden water and acid solution, we investigated the mole ratio of CaO to $Al_2O_3$and the quantitative phase composition for each of Secar 51, 60, 71, and 80 CACs, the starting materials (Table I). The mole ratio was obtained from chemical analysis of the CACs in accordance with

TABLE I CaO/Al_2O_3 ratio and quantitative phase composition of various CAC reactants

CAC	CaO/Al_2O_3 ratio	Phase composition[a]
51	0.72	$C_2AS > CA > CT$
60	0.66	$CA > C_2AS > CT$
71	0.40	$CA \cong CA_2 > C_2AS$
80	0.21	α-$Al_2O_3 > CA \cong CA_2$

[a]C_2AS: $2CaO \cdot Al_2O_3 \cdot SiO_2$; CA: $CaO \cdot Al_2O_3$; CA_2: $CaO \cdot 2Al_2O_3$; CT: $CaTiO_3$.

ASTM-spec. ASTM 618. XRD was used to gain information on phase composition. As shown, the ratio of CaO to Al_2O_3 in the CACs depended on the Secar serial number; namely, the ratio decreased with an increasing serial number. Secar 51 CAC had the highest CaO/Al_2O_3 ratio of 0.72, and Secar 80 had the lowest ratio of 0.21. The XRD data showed that 51 and 60 CACs included three major crystalline phases, monocalcium aluminate ($CaO \cdot Al_2O_3$, CA), gehlenite ($2CaO \cdot Al_2O_3 \cdot SiO_2$, C_2AS) and pervoskite ($CaTiO_3$, CT). 71 CAC was composed of CA, C_2AS, and calcium bialuminate ($CaO \cdot 2Al_2O_3$, CA_2), and 80 CAC had three phases, corundum (α-Al_2O_3), CA, and CA_2. In Table I, the relative quantity of these phases for each CAC was ranked by comparing the total areas of the major XRD *d*-space of CA, CA_2, C_2AS, CT, and α-Al_2O_3 at 0.298, 0.349, 0.285, 0.27, and 0.209 nm, respectively. For 51 CAC, the C_2AS phase was the dominant component, coexisting with the CA phase as the secondary one. By contrast, the principal component of 60 CAC was the CA phase, with the C_2AS as the secondary one. CA and CA_2 were the two major phases of 71 CAC, with one minor phase attributed to C_2AS. The phase composition of the 80 CAC was ranked in the following order; α-$Al_2O_3 > CA \cong CA_2$.

3.2. Phase composition of cements

The focus next concentrated on identifying the crystalline and amorphous phases as reaction products, which are responsible for strengthening the SFCB cements at room temperature. Fig. 1 depicts the XRD patterns, *d*-space ranging from 0.249 to 0.444 nm, for the SFCB cements made with the 51, 60, 71, and 80 CACs. For 51 CAC cements, the diffraction pattern revealed the presence of hybrid phases including three non-reacted components, CA, C_2AS, and CT, originating from the 51 CAC reactant, the quartz and mullite components present in the non-reacted fly ash reactant, and two reaction products attributed to hydroxyapatite [$Ca_5(PO_4)_3(OH)$, HOAp] and boehmite (γ-AlOOH).

Conceivably, both the HOAp and boehmite reaction products were yielded by reactions between NaP and CA at room temperature. In aqueous medium, NaP readily dissolves to form the $NaHPO_4^-$ anion [6]:

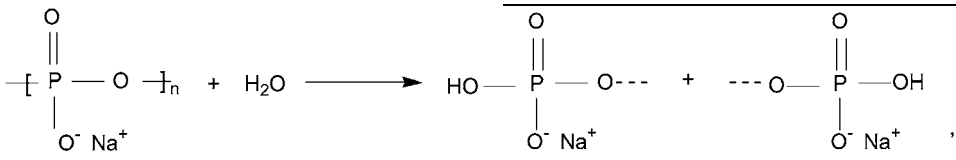

On the other hand, when CA comes into contact with the water, the Ca^{2+} ion is liberated by the hydrolysis of CA phase; $CaO \cdot Al_2O_3 + 4H_2O \rightarrow Ca^{2+} + 2Al(OH)_4^-$ [7]. Thus, the Ca^{2+} cation favorably reacts with $NaHPO_4^-$ as its counter ion to generate a crystalline HOAp; $5Ca^{2+} + 3NaHPO_4^- + H_2O \rightarrow Ca_5(PO_4)_3 \cdot (OH) + 3Na^+ + 4H^-$ [8]. However, there is no evidence whether this reaction occurred directly or indirectly. The uptake of Ca^{2+} from CA phase by $NaHPO_4^-$ left a Ca-depleted CA behind, reflecting the formation of $Al(OH)_4^-$. Although no attempt was made to validate the conversion pathway of $Al(OH)_4^-$ into γ-AlOOH, we assumed that it may take place as follows: $Al(OH)_4^- + H^+ \rightarrow AlH(OH)_4 \rightarrow \gamma\text{-AlOOH} + 2H_2O$. The other way in which HOAp may be formed is by the interactions between NaP and Ca^{2+} liberated from the C_2AS. In this case, the Ca-depleted C_2AS may yield two anionic species, $2Al(OH)_4^-$ and $H_3SiO_4^-$, in an aqueous medium [9]:

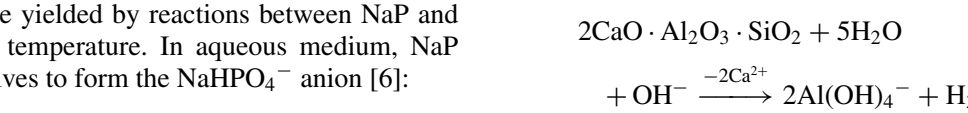

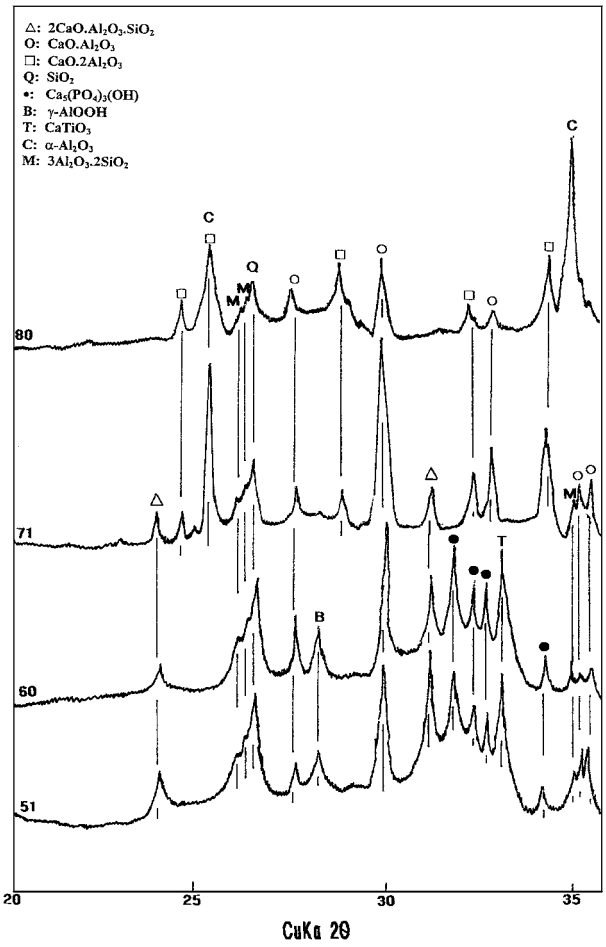

Figure 1 XRD patterns of the SFCB cements made with 51, 60, 71, and 80 CAC at room temperature.

Then, the chemical affinity between these two anions and the Na^+ cations from NaP may generate hydro-aluminosilicates that are zeolite formula: $Na_2O \cdot xAl_2O_3 \cdot ySiO_2 \cdot nH_2O$ [10]. The features of the XRD pattern of cements made with 60 CAC differed from that of the 51 cements; in particular, there was an intensive signal of *d*-spacings related to HOAp, boehmite, and CA, while the intensity of the C_2AS-associated lines declined. Since the CA phase in 60 CAC is the principal component, the 60 CAC-made

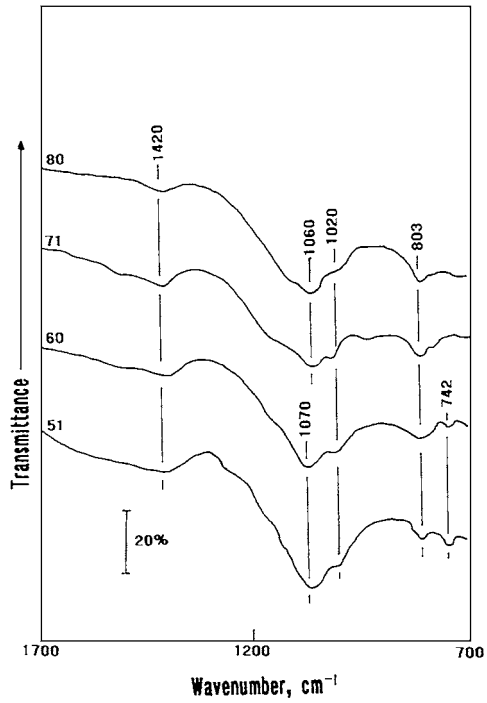

Figure 2 FT-IR spectra for 51, 60, 71, and 80 CAC-made SFCB cements.

cements have more HOAp and boehmite phases as the reaction products, compared to the 51 CAC cements containing the CA as their secondary component. In contrast, no crystalline phases representing reaction products were found in both the 71 and 80 CAC cements. Their XRD tracings showed only the presence of non-reacted C_2AS, CA, CA_2, SiO_2, mullite, and α-Al_2O_3 components, suggesting that the reaction products which bind these CAC grains and fly ash particles into a cohesive mass are essentially amorphous.

To support this information, FT-IR analyses were carried out for the same cements as those used in the XRD study, over the frequency range of 1700–700 cm^{-1} (Fig. 2). The FT-IR spectrum of the 51 cements had five absorption bands at 1420, 1070, 1020, 803, and 742 cm^{-1}. The first band can be ascribed to the stretching vibration of CO_3 in the calcite [11], implying that the cements underwent some carbonation during curing and drying at 110°C. The major contributor to the band at 1070 cm^{-1} is the P-O stretching mode in the HOAp phase [12]. However, the Al-O-H bending mode in the γ-AlOOH also generates a peak near 1070 cm^{-1} [13, 14], so that the strong band at 1070 cm^{-1} is not only due to HOAp, but also encompasses γ-AlOOH. Although the FT-IR curves for each of these CAC reactants are not shown, the spectra of all the reactants indicated two prominent peaks around 1030 and 805 cm^{-1}. Thus, the bands at 1020 and 803 cm^{-1} perhaps belong to the non-reacted CACs. The band detected at 742 cm^{-1} is assigned to the Al-O stretching mode in the γ-AlOOH [14]. The spectral features of the 60 cements closely resembled that of the 51 cements. By comparison, the specific features of the spectra for the 71 and 80 cements were as follows. First is the shift of the band at 1070 cm^{-1}, revealing HOAp, to a low frequency site at 1060 cm^{-1}. Second is the lack of a peak at 742 cm^{-1}, which is due to γ-AlOOH. In the former case, the band at 1060 cm^{-1} may account for the P-O stretching mode in the formation of amorphous dibasic calcium phosphate hydrate, $Ca(HPO_4) \cdot xH_2O$, [15]. The spectra of these cements had a pronounced peak at 3450 cm^{-1}, representing the O-H stretching in its hydrates (data not shown). Assuming that this interpretation is valid, $Ca(HPO_4) \cdot xH_2O$ was formed as the amorphous reaction product by the interactions between Ca^{2+} liberated from the 71 and 80 CACs, and $NaHPO_4^-$ from NaP: $Ca^{2+} + NaHPO_4^- + xH_2O \rightarrow Ca(HPO_4) \cdot xH_2O + Na^+$. Simultaneously, this reaction generates two anionic species, $Al(OH)_4^-$ and $H_3SiO_4^-$ because of the decalcification of CA, CA_2, and C_2AS present in these CACs.

From the XRD and FT-IR data, we summarized the resulting phase compositions encompassing all the reaction products and the remaining non-reacted reactants (Table II).

Table III shows the porosity of these cements cured in an atmospheric environment. The number of pores in the cements depended on what type of CAC reactant was used. The lowest porosity of 24.5% was found in the 71 CAC cements, thereby resulting in the development of a denser microstructure. The next lowest porosity was measured from the cements made with 60 CAC, while a porosity of more than 50% was measured from 51 cements, which allowed the carbonating and acid solutions to permeate through the cement more easily than did the other cement systems.

3.3. Acid resistance of non-carbonated cements

Based upon this information, our experiments centered on assessing the ability of non-carbonated cements

TABLE II Phase compositions for the SFCB cements made with various CACs at room temperature

SFCB cement	Reaction products: Principal phase	Reaction products: Secondary phase	Remaining non-reacted reactant
51	$Ca_3(PO_4)_3(OH)$	γ-AlOOH	$2CaO \cdot Al_2O_3 \cdot SiO_2$, $CaO \cdot Al_2O_3$, $CaO \cdot Al_2O_3$, SiO_2, $3Al_2O_3 \cdot 2SiO_2$, $CaTiO_3$
60	$Ca_3(PO_4)_3(OH)$	γ-AlOOH	$2CaO \cdot Al_2O_3 \cdot SiO_2$, $CaO \cdot Al_2O_3$, $CaO \cdot Al_2O_3$, SiO_2, $3Al_2O_3 \cdot 2SiO_2$, $CaTiO_3$
71	$Ca(HPO_4) \cdot xH_2O$		$2CaO \cdot Al_2O_3 \cdot SiO_2$, $CaO \cdot Al_2O_3$, $CaO \cdot Al_2O_3$, SiO_2, $3Al_2O_3 \cdot 2SiO_2$
80	$Ca(HPO_4) \cdot xH_2O$		$2CaO \cdot Al_2O_3 \cdot SiO_2$, $CaO \cdot Al_2O_3$, $CaO \cdot Al_2O_3$, SiO_2, $3Al_2O_3 \cdot 2SiO_2$, α-Al_2O_3

TABLE III Porosity of SFCB cements made with various CAC reactants at room temperature

SFCB cement	Porosity (%)
51	52.6
60	34.8
71	25.5
80	46.2

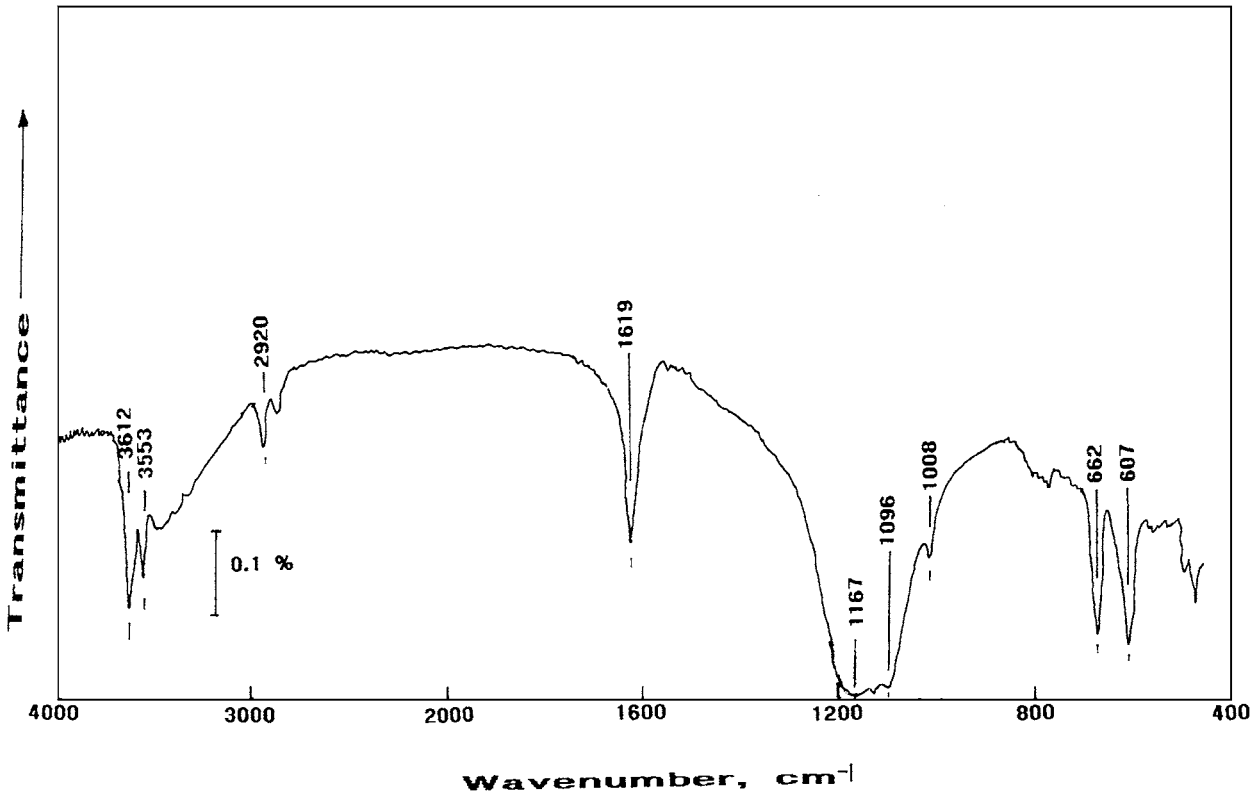

Figure 3 FT-IR spectrum of acid corrosion product deposited on the cement surfaces.

to inhibit the acid corrosion. Thus, we immersed the specimens in the H_2SO_4 solution at 90°C for up to 90 days. In the first 10 days of immersion, we saw that the entire surfaces of all cements are covered rapidly with the less soluble gel corrosion products. We physically removed these corrosion products from the cement surfaces to identify their chemical composition by FT-IR analysis (Fig. 3). The spectral features clearly showed [16] that the acid corrosion product is gypsum gel ($CaSO_4 \cdot 2H_2O$), formed by the reaction between Ca^{2+} leached out from the cements, and the SO_4^{2-} from H_2SO_4: $Ca^{2+} + 2OH^- + SO_4^{2-} + 2H^+ \rightarrow CaSO_4 \cdot 2H_2O$. Hence, when the cements came into contact with the H_2SO_4 solution, the Ca^{2+} cations were rapidly leached out from the cements, and then reacted with H_2SO_4 to deposit gypsum gel scales on the surfaces of cements. Nevertheless, we brushed off the gypsum scales clinging to the outside of the cements before measuring their weight, so that the extent of their acid erosion could be estimated from weight loss. Fig. 4 plots the loss in weight for these cements as a function of exposure time. The data clearly demonstrated that the magnitude of weight loss depended on the CAC species. After 90 days exposure, the lowest weight loss, 28.9%, was observed from the 71 cements; their resistance to acid was the best among the four cements. The second best cement with a weight loss of 34.3%, was that made with the 60 CAC, whereas the 51 CAC cement was the most vulnerable to acid erosion. We also noted, for all the specimens, that their rate of weight loss markedly increased for the first 10 days exposure; beyond that, it progressed gradually. This finding seems to suggest that the reactions between the cement and H_2SO_4 not only lead to the deposition of gypsum scale as the corrosion product on the eroded cement surfaces, but also neutralize the low pH environment surrounding the cements. Further, the gypsum scales might serve as a primary barrier against further acid attack. Relating this finding to the CaO/Al_2O_3 ratio in CACs and the porosity of cements, two factors, (1) low CaO/Al_2O_3 ratio and (2) reduced porosity, seem to play an important role in minimizing a loss in weight of the cement by H_2SO_4 corrosion. For the latter factor, the porosity of the 80 cements was ~81% and ~33% higher than that of the 71 and 60 cements, respectively. Correspondingly, the increase in porosity allows the acid solution to permeate through the cement easily. Thus, although 80 CAC had the lowest CaO/Al_2O_3 ratio in this series, there is no doubt that a high rate of permeability to acid solution promotes the diffusion of more Ca^{2+} ions outwards from the cement surfaces, thereby causing the formation of massive corrosion-induced gypsum scales. From

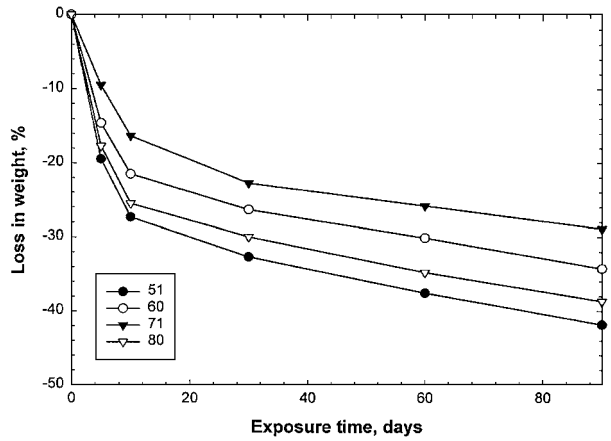

Figure 4 Loss in weight of SFCB cements made with various CACs as a function of exposure time to acid at 90°C.

the above information, the following statement can be conclusively drawn: extending the exposure time leads to a further growth of gypsum scales and also causes spattering of some gypsum scales. Thus, if the gypsum scales were completely scoured off from the cement surfaces, the underlying fresh cements again could be exposed and re-sulfurized to rebuild the protective gypsum layers. In other words, the consumption of Ca from the cements is inversely proportional to the amount of gypsum. Relative to the high rate of hydrolysis, the source of the consumed Ca is more likely to be associated with the remaining non-reacted CA, CA_2, and C_2AS components, rather than with the reaction products, which are relatively inert to acid. Hence, as the entire cement surfaces were fully covered with gypsum scales, any further chemical and hydration reactions of the Ca-destitute and non-destitute reactive components in the cements create more reaction products. This is of important concern to preventing the deficiency of Ca in the cements.

To substantiate the above concept, the hydrated reaction products formed in the superficial layer of the cements beneath the gypsum scales were carefully identified. The superficial layer with a depth of 1–2 mm for the 90-day-exposed cements was scraped off with a diamond-edged scrubber. These powder samples were dried at 100°C for XRD and FT-IR analyses. Fig. 5 depicts the XRD tracings of these exposed cements. When the diffraction pattern of 51 cement was compared with that of unexposed cements, there were two

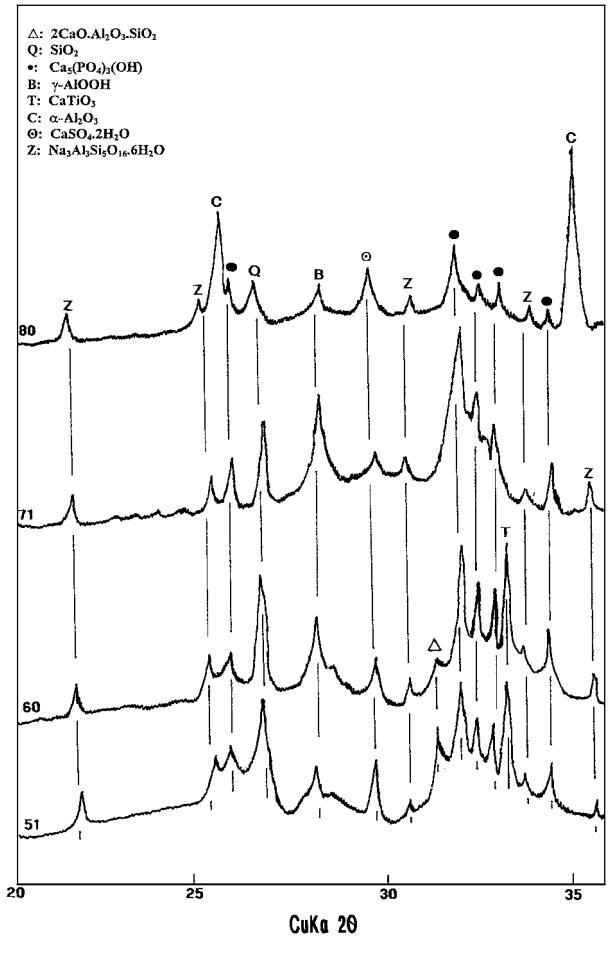

Figure 5 XRD tracings for 51, 60, 71, and 80 SFCB cements after exposure for 90 days to 90°C H_2SO_4 solution.

distinctive features. One difference was the appearance of two new crystalline reaction products as the major phases, the Na-P type zeolite, $Na_3Al_3Si_5O_{16} \cdot 6H_2O$ and gypsum, and the other was the disappearance of CA and mullite reactants, along with a striking decay of the intensity of the C_2AS-related line. The elimination and diminution of these reactants can be surmised, as the reactions of these reactants were completed or partially completed. The Na-P type zeolite might be yielded by the reactions of Na^+ from NaP with both mullite and the Ca-depleted C_2AS. The pattern also included a strong line of CT, seemingly suggesting that the reactivity of CT with NaP is very poor. The pattern of the 60 cements somewhat differed from that of the 51 cements. Among the differences are: (1) the increased line intensity of the HOAp- and boehmite-related *d*-spacings and (2) the diminished line of the C_2AS phase. The growth of a *d*-spacing line reflects an increase in the amount of its particular crystal phase. Thus, the formation of more HOAp and boehmite in the 60 cement bodies may signify that there is a great deal of the CA phase in the 60 CAC reactant, namely, most of the CA reacted with NaP to form two reaction products, HOAp and boehmite. The further growth of lines for the HOAp and boehmite phases were observed in the diffraction pattern of the 71 cements, implying that the CA and CA_2 phases in the 71 CAC were transformed into these reaction products during exposure. In fact, there are no *d*-spacings related to CA and CA_2, which were detected as the major phases in the unexposed cements. From this information, the transformation of CA and CA_2 into these reaction products was completed through the following hypothetical reaction pathways:

Hydrolysis of reactants:

$$CaO \cdot Al_2O_3 + 4H_2O \rightarrow Ca^{2+} + 2Al(OH)_4{}^-,$$
$$CaO \cdot 2Al_2O_3 + 7H_2O + 2OH^- \rightarrow Ca^{2+} + 4Al(OH)_4{}^-,$$
$$-[-NaPO_3-]_n- + nH_2O \rightarrow nNaHPO_4{}^- + nH^+,$$

Interactions:

$$Ca^{2+} + NaHPO_4{}^- + nH_2O \rightarrow Ca(HPO_4) \cdot xH_2O,$$
$$Ca(HPO_4) \cdot xH_2O + 4Ca^{2+} + 2NaHPO_4{}^- \rightarrow Ca_5(PO_4)_3\,(OH) + 2Na^+ + xH^+ + yOH^-,$$
$$Al(OH)_4{}^- + H^+ \rightarrow AlH(OH)_4 \rightarrow \gamma\text{-}AlOOH + 2H_2O.$$

In the induction stage of reactions described as hydrolysis of reactants, the CA and CA_2 phases dissociate into two counter ionic species, Ca^{2+} and $Al(OH)_4{}^-$. Simultaneously, the NaP is converted into another two counter hydrolysates, $NaHPO_4{}^-$ and H^+, in an aqueous medium. These counter ionic reactants liberated from CA, CA_2, and NaP begin to interact between each other in the following interaction stage; namely, Ca^{2+} reacts with $NaHPO_4{}^-$ counter ion to yield the amorphous $Ca(HPO_4) \cdot xH_2O$ compound as the intermediate reaction product. A further chemical and hydration reaction of $Ca(HPO_4) \cdot xH_2O$ with Ca^{2+} and $NaHPO_4{}^-$ leads to the formation of crystalline $Ca_5(PO_4)_3(OH)$ as the final reaction product. On the other hand, the uptake of H^+ by the $Al(OH)_4{}^-$ generates $AlH(OH)_4$ as the intermediate derivative. Then, the dehydration of $AlH(OH)_4$ results in its phase transition into γ-AlOOH. The x-ray tracing

TABLE IV Phase compositions for 51, 60, 71, 80 SFCB cements after exposure for 90 days to 90°C H_2SO_4 solution

SFCB cement	Reaction products		Remaining non-reacted reactant
	Principal phase	Secondary phase	
51	$Ca_3(PO_4)_3(OH)$	γ-AlOOH, $CaSO_4 \cdot 2H_2O$, $Na_3Al_3Si_5O_{16} \cdot 6H_2O$	$2CaO \cdot Al_2O_3 \cdot SiO_2$, SiO_2, $CaTiO_3$
60	$Ca_3(PO_4)_3(OH)$, γ-AlOOH	$CaSO_4 \cdot 2H_2O$, $Na_3Al_3Si_5O_{16} \cdot 6H_2O$	$2CaO \cdot Al_2O_3 \cdot SiO_2$, SiO_2, $CaTiO_3$
71	$Ca_3(PO_4)_3(OH)$, γ-AlOOH	$CaSO_4 \cdot 2H_2O$, $Na_3Al_3Si_5O_{16} \cdot 6H_2O$	SiO_2
80	$Ca_3(PO_4)_3(OH)$, γ-AlOOH, $CaSO_4 \cdot 2H_2O$	$Na_3Al_3Si_5O_{16} \cdot 6H_2O$	SiO_2, α-Al_2O_3

TABLE V Gain in weight of SFCB cements after exposure for 20 days to 4 wt% $NaHCO_3$-laden water at 90°C

CAC	Gain in weight (%)
51	4.4
60	3.8
71	2.4
80	0.3

also showed the presence of the zeolite phase coexisting with HOAp and boehmite. As described earlier, zeolite is formed by the uptake of Na^+ from NaP by mullite and decalcified C_2AS. Again, no non-reactive phases such as CA and CA_2 were found from the XRD pattern of the 80 cements. All these phases appeared to be converted into HOAp and boehmite. The pattern also showed the persistence of the prominent line of the α-Al_2O_3 phase, reflecting its inertness to react with NaP.

Furthermore, the intensity of HOAp and boehmite lines was weak compared to that of the other cements, demonstrating that the amount of the CA and CA_2 components as the sources of these reaction products was relatively small.

Based upon the information described above, the phase compositions for these SFCB cements after exposure for 90 days to acid are summarized in Table IV.

Nevertheless, three reaction products, HOAp, boehmite, and Na-P type zeolite, were formed beneath the gypsum scale layers during the exposure to acid. Although we did not study the susceptibility of these reaction products to H_2SO_4, we believe that they play an essential role in preventing further acid corrosion of the cements.

3.4. Acid resistance of carbonated cements

Based on the information gained regarding the acid corrosion and inhibition of the SFCB cements submersed directly in a hot H_2SO_4 solution, our study now shifted to investigating the ability of the carbonated cements to withstand acid attack. Table V shows the changes in weight of the carbonated cements after exposure for 20 days to 90°C 4 wt% $NaHCO_3$-laden water. All the exposed specimens gained weight. The highest gain of 4.4% was seen in the 51 cements, whereas the gain was minimal in the 80 cement. Relating this result to the CaO/Al_2O_3 ratio of CACs, the weight gain caused by the carbonation of the cements was associated with this ratio. The increased ratio corresponds to an increment of weight gain. This information was supported by the XRD and FT-IR analyses of the powder samples taken from the superficial layer (~1 mm thick) of the 20-day carbonated cements. The XRD data (Fig. 6) clearly verified that the intensity of the line related to

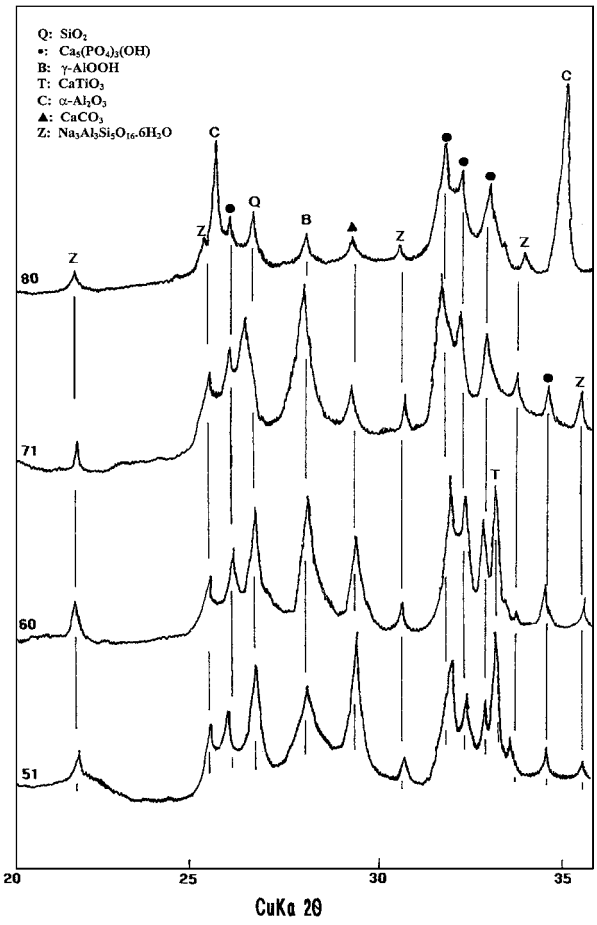

Figure 6 XRD tracings for various 20-day carbonated SFCB cements.

calcite, $CaCO_3$, formed by the carbonation of the cements tends to decline with a decreasing CaO/Al_2O_3 ratio. Compared to that of the 51 cements, the noticeable decay of the *d*-spacing line of calcite was obtained from the 80 cement made with the lowest ratio. Also, the data for all the cements revealed that three reaction products were formed: HOAp, boehmite, and Na-P type zeolite. All the reactive components, such as CA, CA_2, C_2AS, and mullite, except for perovskite, $CaTiO_3$, were eliminated because the reaction between these reactive components and NaP was completed during the exposure to carbonating solution. Furthermore, the patterns for each of these cements closely resembled those of the same cements after exposure to acid, demonstrating that the crystalline phase composition similar to that formed in the 90-day acid-exposed cements was assembled in the carbonated cements.

Fig. 7 compares the FT-IR spectral features of these cements over the frequency range of 1700 to 700 cm^{-1}. The spectrum of the 51 cements had four absorption bands at 1472, 1420, 1070, and 742 cm^{-1}. As described earlier in this paper, the band at 1070 cm^{-1} is

TABLE VI Phase compositions for 51, 60, 71, 80 SFCB cements after exposure for 20 days to 90°C 4 wt% $NaHCO_3$-laden water

SFCB cement	Reaction products		Remaining non-reacted reactant
	Principal phase	Secondary phase	
51	$Ca_3(PO_4)_3(OH)$, $CaCO_3$	$\gamma-AlOOH$, $Ca_3(PO_4)_3[OH_{x-y}(CO_3)_y]$, $Na_3Al_3Si_5O_{16}\cdot 6H_2O$	SiO_2,$CaTiO_3$
60	$Ca_3(PO_4)_3(OH)$, γ-AlOOH, $CaCO_3$	$Ca_3(PO_4)_3[OH_{x-y}(CO_3)_y]$, $Na_3Al_3Si_5O_{16}\cdot 6H_2O$	SiO_2, $CaTiO_3$
71	$Ca_3(PO_4)_3(OH)$, γ-AlOOH	$Ca_3(PO_4)_3[OH_{x-y}(CO_3)_y]$, $CaCO_3$, $Na_3Al_3Si_5O_{16}\cdot 6H_2O$	SiO_2
80	$Ca_3(PO_4)_3(OH)$	$Ca_3(PO_4)_3[OH_{x-y}(CO_3)_y]$, γ-AlOOH, $CaCO_3$, $Na_3Al_3Si_5O_{16}\cdot 6H_2O$	SiO_2, α-Al_2O_3

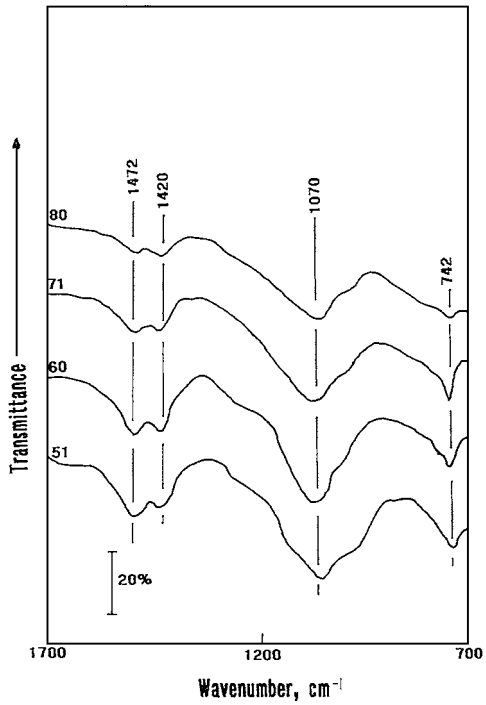

Figure 7 FT-IR spectra for 20-day carbonated SFCB cements.

attributed to the HOAp and boehmite phases, especially the former one. The latter phase also refers to the band to 742 cm^{-1}. Since the CO_3-related absorption bands commonly arise in the frequency range from 1420 to 1490 cm^{-1} [17], it appears that two bands at 1420 and 1472 cm^{-1} belong to the different carbonated components. According to literature [18], the bands near 1460 and 1500 cm^{-1} were due to the formation of CO_3-incorporated HOAp structure generated by substituting CO_3^{2-} for OH^-. Thus, a possible contributor to the latter band is the formation of CO_3-intercalated HOAp, $Ca_5(PO_4)_3[OH_{x-y}(CO_3)_y]$. For all other cements, only differing in spectral features, compared to that of the 51 cements, was the intensity of these CO_3-related bands. Their intensity of the 60 cements appears to be reduced somewhat, and a further reduction was observed from the 71 cements. Moreover, their intensity of the 80 cements had become even lower. This information strongly supported the results from the XRD study. The rate of carbonation attributed to the formation of calcite and CO_3-intercalated HOAp in the cements is correlated directly with the CaO/Al_2O_3 ratio of CAC reactants; namely, its rate increases with an increasing CaO/Al_2O_3 ratio.

From the XRD and FT-IR results, Table VI summarizes the phase compositions for these cements after exposure for 20 days to 4 wt% $NaHCO_3$-laden water at 90°C.

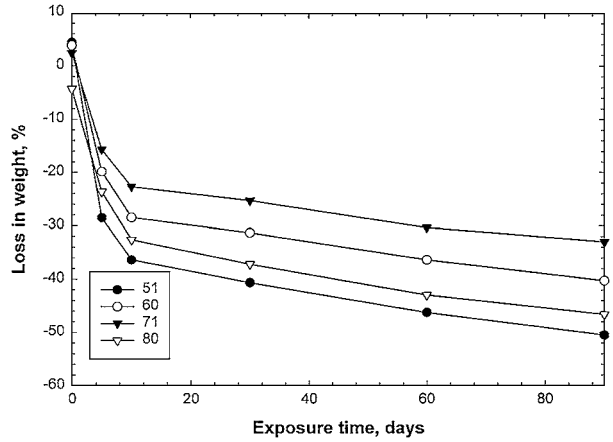

Figure 8 Loss in weight of carbonated SFCB cements as a function of exposure time to acid at 90°C.

These carbonated cements were immersed for up to 90 days in the 90°C acid solution, and the loss in weight of these cements was measured to obtain information on their susceptibility to acid corrosion. Fig. 8 plots their changes in weight against the times of exposure. As expected, all the cements underwent the H_2SO_4 corrosion, thereby resulting in the deposition of gypsum scales on their surfaces. The gypsum scales were rapidly deposited during exposure for 10 days, and then served to protect the cements from further acid attack. The formation of the protective gypsum barrier is the reason why the loss in weight of the cements was gradual after the first 10 days. This phenomenon was quite similar to that seen during the exposure to acid of non-carbonated cements. Again, the surfaces of exposed cements were brushed to remove any gypsum, and were weighted to measure the loss in weight. After 90 days exposure, the 71 cements indicated the lowest weight loss of 33%. However, this value was ~14% higher than that of the non-carbonated specimens after the same exposure time. Similarly, the weight loss for all the other cements was ~17% greater over those of the non-carbonated ones. This information strongly suggested that the carbonated cements become more vulnerable to acid corrosion.

The magnitude of the resistance of these cements to acid was ranked in the following order; 71 > 60 > 80 > 51, the same as the ranking of the non-carbonated cements.

Fig. 9 illustrates the XRD tracings for the powder samples scoured off from the surfaces of the 90-day exposed cements after removing the gypsum scales. A specific characteristic of the diffraction pattern for the 51 cements was the presence of a strong *d*-spacing attributed to gypsum; meanwhile, there was no calcite-related XRD line. The features of the overall

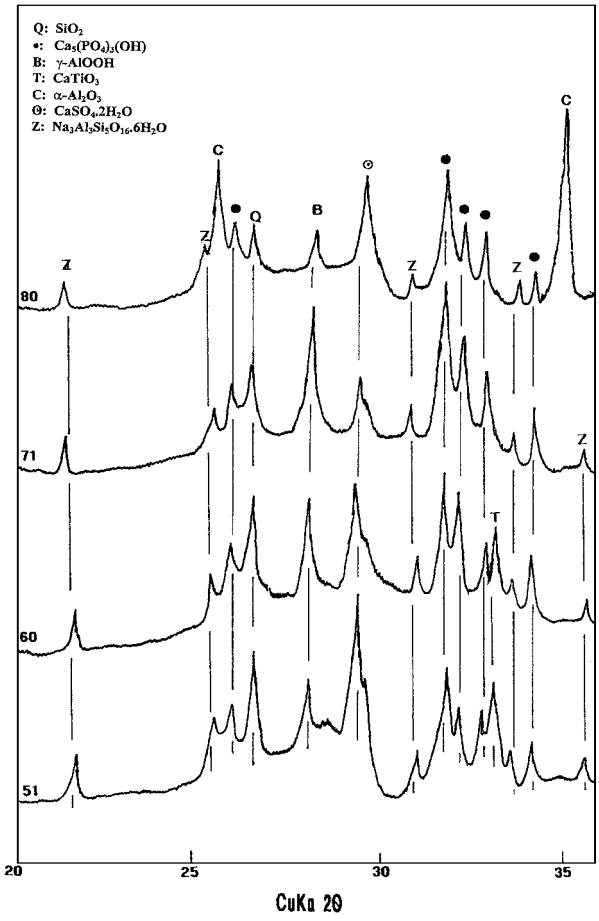

Figure 9 XRD analyses for various carbonated SFCB cements after exposure for 90 days to acid.

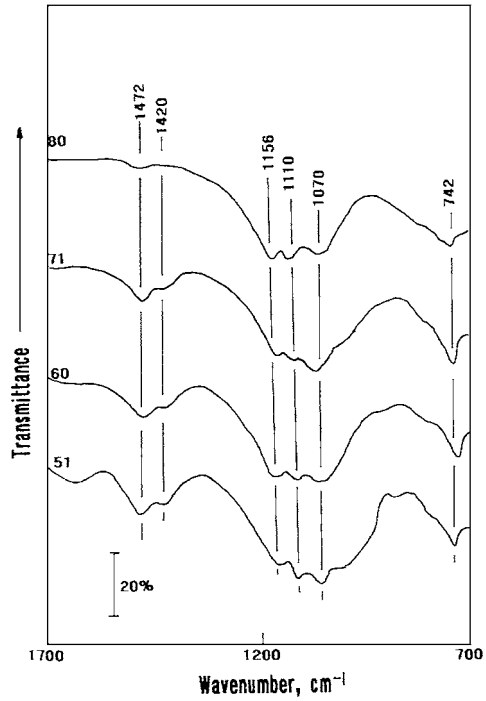

Figure 10 FT-IR analyses for carbonated SFCB cements after 90 days exposure to acid.

pattern were almost the same as that of the carbonated one; there were three reaction products, HOAp, boehmite, and Na-P type zeolite, and two non-reacted components, quartz and pervoskite. This information substantiates that all the calcite phase formed by the carbonation of the cements was eventually transformed into the gypsum through the interactions between calcite and H_2SO_4: $CaCO_3 + H_2SO_4 + H_2O \rightarrow CaSO_4 \cdot 2H_2O + CO_2 \uparrow$. Although the phase composition of the 60 cements was similar to that of the 51 cements, there were two distinctive differences in pattern. One was a weakening line intensity of gypsum and the other was a conspicuous growth of the HOAp and boehmite lines. A possible interpretation of these results was that the amount of gypsum as a corrosion product was much less than that of the 51 cements, whereas well-formed HOAp and boehmite phases were yielded in the 60 cement bodies. A further increase in the intensity of the lines of HOAp and boehmite phases together with a weakening of the gypsum peak was obtained from the 71 cements, indicating that the formation of more HOAp and boehmite imparts better protection of cements against acid corrosion. By contrast, the line intensity of the HOAp and boehmite phases for the 80 cements was considerably lower, implying that the amount of these phases as the corrosion-protective reaction products is much less than that of the 71 cements. A dearth of these important reaction products might increase in the rate of acid erosion. Fig. 10 illustrates the FT-IR spectra of the same samples as those used in the XRD analysis. Compared to those of the carbonated cements before acid exposure, there are striking changes in the spectral feature of these exposed cements. The calcite-associated CO_3 band at 1420 cm^{-1} for the 51, 60, and 71 cements became a shoulder peak, while it was eliminated from the 80 cement. Correspondingly, for all the cements, the peak intensity of the gypsum-related bands at 1156 and 1110 cm^{-1} markedly increased, indicating that the calcite has a strong chemical affinity with H_2SO_4 so promoting the calcite $\rightarrow$ gypsum phase transition. On the other hand, there were no marked changes in peak intensity of the other carbonation species at 1472 cm^{-1}, demonstrating that the susceptibility of CO_3-intercoalted HOAp to the reaction with H_2SO_4 was very little, if any.

From the integration of XRD and FT-IR data, Table VII summarizes the phase compositions for these carbonated cements after exposure to acid.

TABLE VII Phase compositions for carbonated 51, 60, 71, 80 SFCB cements after exposure for 90 days to 90°C acid

SFCB cement	Reaction products		Remaining non-reacted reactant
	Principal phase	Secondary phase	
51	$CaSO_4 \cdot 2H_2O$, $Ca_3(PO_4)_3(OH)$	$\gamma-AlOOH$, $Ca_3(PO_4)_3[OH_{x-y}(CO_3)_y]$, $Na_3Al_3Si_5O_{16} \cdot 6H_2O$	SiO_2, $CaTiO_3$
60	$Ca_3(PO_4)_3(OH)$, γ-AlOOH, $CaSO_4 \cdot 2H_2O$	$Ca_3(PO_4)_3[OH_{x-y}(CO_3)_y]$, $Na_3Al_3Si_5O_{16} \cdot 6H_2O$	SiO_2, $CaTiO_3$
71	$Ca_3(PO_4)_3(OH)$, γ-AlOOH	$Ca_3(PO_4)_3[OH_{x-y}(CO_3)_y]$, $CaSO_4 \cdot 2H_2O$, $Na_3Al_3Si_5O_{16} \cdot 6H_2O$	SiO_2
80	$Ca_3(PO_4)_3(OH)$, $CaSO_4 \cdot 2H_2O$	$Ca_3(PO_4)_3[OH_{x-y}(CO_3)_y]$, γ-AlOOH, $Na_3Al_3Si_5O_{16} \cdot 6H_2O$	SiO_2, α-Al_2O_3

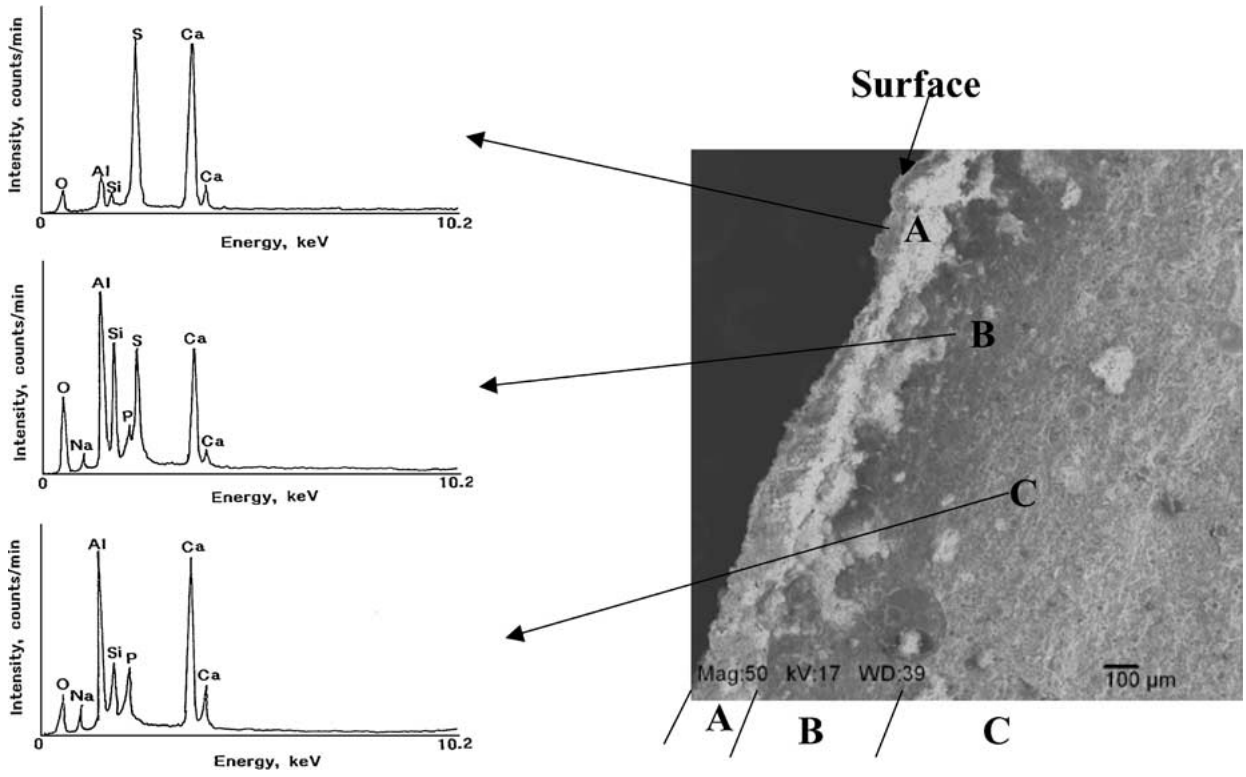

Figure 11 SEM-EDX exploration for the fractured surfaces of carbonated 71 SFCB cement after exposure for 90 days to acid.

To support the above information, we explored the microstructure developed in the carbonated cement after exposure to acid by SEM and EDX. Since the most effective CAC reactant in alleviating the acid erosion of the SFCB cement is 71, this cement was employed for exploring the development of microstructures. Fig. 11 shows the SEM microphotograph of the fractured surfaces for the carbonated 71 SFCB cement after exposure for 90 days to H_2SO_4. The SEM image revealed three distinctive layers, a depth of $\sim$200 μm from the top surfaces denoted as "A" layer, an $\sim$440 μm in depth from "A" layer marked as "B" layer, and the "C" layer at a distance of $>$640 μm away from the surfaces. For the "A" layer, the EDX spectrum coupled with this SEM image included two prominent peaks from S and Ca as the dominant elements and a very weak signal for O, Al, and Si. These dominant elements are attributed to the formation of gypsum. The Al and Si in conjunction with O may originate from the boehmite and quartz.

Nevertheless, the top layer with 200 μm thick appears to be occupied by the gypsum. In contrast, the spectral feature of EDX for the "B" layer was characterized by appearance of five major peaks with O, Al, Si, S, and Ca, while the Na and P are present as miner peaks. This finding seems to suggest that this layer consists of three principal components, boehmite, quartz, and gypsum, and two secondary components, HOAp and zeolite. Thus, the "B" layer can be interpreted as the transition zone. In fact, the EDX spectrum in the "C" layer showed a typical elemental distribution of original SFCB cement; namely, the two strong signals, Al and Ca, attributed to the beohmite and HOAp, as the principal reaction products. No signal of S element originating from the gypsum was found in this layer.

As a result, top gypsum layer with $\sim$640 μm in conjunction with the γ-AlOOH and quartz as minor phases seems to act as a protective barrier in abating further acid erosion. Such a protection led to the formation of HOAp and γ-AlOOH as the well-crystallized major reaction products in the SFCB cement during exposure to acid.

4. Conclusion

We are attempting to formulate a sodium polyphosphate-modified fly ash/calcium aluminate blend (SFCB) geothermal well cements with the advanced anti-carbonation and anti-acid corrosion properties. To increase our knowledge of the chemistry of the SFCB cements, we investigated the role of the calcium aluminate cement (CAC) reactants in the SFCB system in minimizing the rate of carbonation and in inhibiting H_2SO_4 corrosion. As a result, CAC containing two major phases, monocalcium aluminate (CA) and calcium bialuminate (CA_2), and a moderate CaO/Al_2O_3 ratio of 0.4 was identified to be the most effective one in satisfying the above requirements. One important factor in abating carbonation and acid attack was a sufficiently low porosity of 25.5%, which diminishes a permeability of carbonating and acid solutions through the cements. However, the remaining non-reacted CA and CA_2 components underwent the carbonation to form calcite, which was susceptible to the reaction with H_2SO_4. The reactions between the calcite and H_2SO_4 led to the deposition of gypsum-gel scales as the acid corrosion product on the cement's surfaces. Although the gypsum scale clinging to the cements was thought to be the major element governing the loss in weight, it served in neutralizing the low pH environment surrounding the cements. Such neutralization by a passive gypsum layer not only protected the cement from an acid corrosion, but

also promoted the chemical and hydration reactions of sodium polyphosphate (NaP) with CA, CA_2, and fly ash to yield three crystalline phases, hydroxyapatite, boehmite, and Na-P type zeolite, as the reaction products. These reaction products were relatively insensitive to acid attack, so protecting the cements from further acid corrosion. The acid corrosion-inhibiting mechanisms of the carbonated SFCB cements can be represented in the following two steps. The first step is the passivation and environmental neutralization by the deposition of gypsum corrosion product on the cement surfaces, and the second one is the formation of these well-crystallized reaction products beneath the protective gypsum layer.

Acknowledgments

This program report, issued by Raymond LaSala (Program Manager, DOE Office of Wind and Geothermal Technologies), was performed under the auspices of the US Department of Energy Washington, DC, under Contract No. DE-AC02-98CH10866.

References

1. T. SUGAMA, N. R. CARCIELLO, T. M. NAYBERG and L. E. BROTHERS, *Cem. Concr. Res.* **25** (1995) 1305.
2. T. SUGAMA, *Adv. Cem. Res.* **9** (1997) 65.
3. *Idem.*, *Cem. Concr. Res.* **26** (1996) 1661.
4. L. WEBER, E. EMERSION, K. HARRIS and L. E. BROTHERS, *Geothermal Resource Council Transaction* **22** (1998) 25.
5. T. SUGAMA, L. WEBER and L. E. BROTHERS, *Cem. Concr. Res.* **29** (1999) 1969.
6. F. G. R. GIMBLETT, "Inorganic Polymer Chemistry" (Butterworths, London, 1963) p. 336.
7. C. E. HARVIE and J. H. WEARE, *Geochim. Cosmochim. Acta.* **44** (1980) 981.
8. Z. JIN and J. HEO, *J. Mater. Sci. Lett.* **17** (1998) 633.
9. E. J. REARDON, *Cem. Concr. Res.* **20** (1990) 175.
10. D. M. ROY, M. R. SILSBEE and D. WOLFE-CONFER, in "Specialty Cements with Advanced Properties," edited by B. E. Scheetz, A. G. Landers, I. Odler and H. Jennings (Materials Research Society, MRS 1990) Vol. 179, p. 203.
11. R. A. NYQUIST and R. O. KAGAL, "Infrared Spectra of Inorganic Compounds" (Academic Press, New York, 1971) p. 79.
12. T. SUGAMA, M. ALLAN and J. M. HILL, *J. Amer. Ceram. Soc.* **75** (1992) 2076.
13. P. H. COLOMBAN, *J. Mater. Sci. Lett.* **7** (1988) 1324.
14. G. K. PRIYA, P. PADMAJA, K. G. K. WARRIER, A. D. DAMODARAN and G. ARULDHAS, *ibid.* **16** (1997) 1584.
15. D. E. C. CORBRIDGE and E. J. LOWE, *J. Chem. Soc.* (1954) 269.
16. R. A. NYQUIST and R. O. KAGAL, "Infrared Spectra of Inorganic Compounds" (Academic Press, New York, 1971) p. 269.
17. L. J. BELLANY, "The Infra-Red Spectra of Complex Molecules" (Chapman and Hall, London, 1975) p. 386.
18. M. NAGAI, T. SAEKI and T. NISHINO, *J. Amer. Ceram. Soc.* **73** (1990) 1456.

Received 5 November 2001
and accepted 11 April 2002